Impact of physical processes on the seasonal distribution of the fugacity of CO2 in the western tropical Atlantic

Nathalie Lefèvre, Domingos F. Urbano, Francis Gallois, Denis Diverrès

AGU PUBLICATIONS

JGR

Journal of Geophysical Research: Oceans

RESEARCH ARTICLE

10.1002/2013JC009248

Key Points:
- Seasonal CO_2 maps from synoptic cruises are produced
- Surface fCO_2 is mainly driven by temperature and salinity
- The equatorial source of CO_2 is decreasing or constant over time

Correspondence to:
N. Lefèvre,
nathalie.lefevre@locean-ipsl.upmc.fr

Citation:
Lefèvre, N., D. F. Urbano, F. Gallois, and D. Diverrès (2014), Impact of physical processes on the seasonal distribution of the fugacity of CO_2 in the western tropical Atlantic, *J. Geophys. Res. Oceans*, *119*, 646–663, doi:10.1002/2013JC009248.

Received 3 JULY 2013
Accepted 31 DEC 2013
Accepted article online 8 JAN 2014
Published online 4 FEB 2014

Impact of physical processes on the seasonal distribution of the fugacity of CO_2 in the western tropical Atlantic

Nathalie Lefèvre[1,2], Domingos F. Urbano[3], Francis Gallois[4], and Denis Diverrès[5]

[1]IRD LOCEAN, Université Pierre et Marie Curie, UMR 7159, Paris, France, [2]LaboMar, Instituto de Ciências do Mar, Fortaleza, Brazil, [3]CPTEC (Centro de Previsão de Tempo e Estudos Climáticos), INPE National Institute for Space Research (Instituto Nacional de Pesquisas Espaciais), São Paulo, Brazil, [4]US IMAGO, Institut de Recherche pour le Developpement Nouméa, Nouvelle Calédonie, France, [5]US IMAGO, Centre IRD de Bretagne, Plouzané, France

Abstract The fugacity of CO_2 (fCO_2) has been measured underway during three quasi-synoptic cruises in the western tropical Atlantic in March/April 2009 and July/August 2010 in the region 6°S–15°N, 52°W–24°W. The distribution of fCO_2 is related to the main features of the ocean circulation. Temperature exerts a dominant control on the distribution of fCO_2 in March/April whereas salinity plays an important role in July/August due to the more developed North Equatorial Countercurrent (NECC) carrying Amazon water and to the high precipitation associated with the presence of the Intertropical Convergence Zone (ITCZ). The main surface currents are characterized by different fCO_2. Overall, the NECC carries less saline waters with lower fCO_2 compared to the South Equatorial Current (SEC). The North Equatorial Current (NEC) is usually characterized by CO_2 undersaturation in winter and supersaturation in summer. Using empirical fCO_2-SST-SSS relationships, two seasonal maps of fCO_2 are constructed for March 2009 and July 2010. The region is a sink of CO_2 of 0.40 mmol $m^{-2}d^{-1}$ in March, explained by the winter cooling in the northern hemisphere, whereas it is a source of CO_2 of 1.32 mmol $m^{-2}d^{-1}$ in July. The equatorial region is a source of CO_2 throughout the year due to the upwelling supplying CO_2-rich waters to the surface. However, the evolution of fCO_2 over time, determined from all the available cruises in a small area, 1°S–1°N, 32°W–28°W, suggests that the source of CO_2 has decreased in February-March from 1983 to 2011 or has remained constant in October-November from 1991 to 2010.

1. Introduction

The tropical Atlantic is characterized by high fugacity of carbon dioxide (fCO_2) and, as a consequence, it is a source of CO_2 for the atmosphere [e.g., *Goyet et al.*, 1998]. The variation of this source of CO_2 over time, under increasing atmospheric CO_2, remains difficult to assess. *Goyet et al.* [1998] compared the WOCE section A15 cruise made in April–May 1994 to the FOCAL cruises of 1982–1984 [*Andrié et al.*, 1986] and concluded that the source of CO_2 decreased over that time period, whereas *Oudot et al.* [1995], comparing the CITHER 1 cruise made in January–March 1993 to the same FOCAL cruises, concluded that the source of CO_2 increased. A possible explanation for their different conclusions might be the strong dynamical processes of the region and the different months of the year they considered.

The western tropical Atlantic is affected by the Amazon River discharge and by the seasonal migration of the Intertropical Convergence Zone (ITCZ) associated with the atmospheric convective belt (i.e., rain) being both sources of freshwater. This region is also an important site for interhemispheric heat exchange through a complex system of surface currents around the equator and due to the convergence of northern and southern water masses [*Stramma and Schott*, 1999]. Using the large number of surface drifters launched in the global oceans in the last two decades, features of the time-mean circulation in the tropical Atlantic Ocean and its seasonal variations at high resolution have being described [*Lumpkin and Garzoli*, 2005; *Urbano et al.*, 2008]. The combination of circulation data with physical and chemical water properties (i.e., temperature, salinity, dissolved oxygen) is important to trace water masses origins and pathways.

Urbano et al. [2008] used surface velocities together with vertical sections of conductivity-temperature-depth (CTD) and acoustic Doppler current profiler (ADCP) to describe the water masses distribution and ocean circulation along 38°W. The ship data used spanned from 1998 to 2006 as part of the PIRATA (Prediction and Research moored Array in the Atlantic) program [*Bourlès et al.*, 2008]. They showed that waters

from the North Atlantic occupy the region north of 11°N. South of it there is the mixed Equatorial Water, which has a contribution from the south Atlantic through the North Brazil Current (NBC) retroflection, from the eastern Atlantic through the South Equatorial Current (SEC), and also from the North Atlantic through the North Equatorial Current (NEC). The eastward North Equatorial Countercurrent (NECC) carries mostly the Equatorial Water eastward. In this work, we use a combination of surface circulation data with underway fCO_2 measurements to understand the CO_2 distribution and its variability in the tropical Atlantic.

The fCO_2 varies from one current system to another. One particular feature of the tropical Atlantic is the difference between the SEC, where high fCO_2 values are encountered, and the NECC characterized by lower fCO_2 values leading to a north south gradient of fCO_2 [*Lefèvre et al*., 2010; *Oudot and Andrié*, 1986]. Although the tropical Atlantic is a source of CO_2, regional sinks of this gas have been reported in its western part. The impact of the Amazon discharge on CO_2 was evidenced by *Ternon et al*. [2000] and later confirmed by *Körtzinger* [2003]. In addition to the dilution effect, *Cooley et al*. [2007] identified, in the Amazon plume, a net community production supported by diazotrophs that takes up CO_2 from the atmosphere. This biological drawdown causes an inorganic carbon deficit that outlasts the physical structure of the Amazon plume [*Cooley and Yager*, 2006]. Large oceanic rings are formed by the retroflection of the North Brazil Current (NBC) and entrain river-influenced shelf water northward along the South American coast and eastward into the NECC. Enhanced phytoplankton production associated with the nutrient-rich Amazon discharge can be observed in near-surface chlorophyll from satellite [*Fratantoni and Glickson*, 2001]. The Amazon River is highly supersaturated with respect to CO_2 because of respiration and degradation of organic matter [*Mayorga et al*., 2005; *Richey et al*., 2002]. When the water mixes with oceanic water, the turbidity decreases and the high levels of nutrients supplied by the river creates strong blooms of diatoms [*Subramaniam et al*., 2008]. The effect of the Amazon plume can be observed very far from the river mouth [*Chen et al*., 2012]. Transported by the NECC, Amazon waters could be observed as far as 25°W in October 1995 [*Lefèvre et al*., 1998]. These mechanisms can then alter the tropical Atlantic source of CO_2. However, it remains difficult to quantify this river impact on the CO_2 budget because of the high variability of seasonal discharge, ITCZ migration, and the complex ocean circulation characterized by several eddies [*Hu et al*., 2004]. Regular observations are needed to determine the extent of sink area as well as the drivers of the CO_2 variability in this region. Identifying the processes affecting the CO_2 distribution will help in understanding and predicting the changes of CO_2 concentration in surface seawater.

In the western tropical Atlantic, the temporal and spatial coverage of fCO_2 is still too sparse to determine the seasonal variability of fCO_2. Empirical relationships between fCO_2 and relevant parameters are useful to interpolate sparse data. Empirical fCO_2-Sea Surface Temperature (SST) relationships have been widely used to reconstruct fCO_2 in several regions of the ocean [e.g., *Lefèvre and Taylor*, 2002; *Olsen et al*., 2003; *Park and Wanninkhof*, 2012; *Stephens et al*., 1995] to obtain estimates of CO_2 in a given region or to reconstruct fCO_2 in order to assess trends.

Here we present the fCO_2 surface distribution from underway measurements made during the PIRATA BR XI in 2009 and PIRATA BR XII in 2010 cruises along 38°W, and along the track of two merchant ships sailing east (voyages of the *Rio Blanco*) and west (voyages of the *MN Colibri*) of the PIRATA cruises. All these cruises have been performed at two different seasons (March–April 2009 and July–August 2010) providing an almost synoptic view of the western tropical Atlantic between 6°S and 15°N in the longitudinal range 52°W–24°W. The processes affecting the variability of fCO_2 are analyzed from surface velocity fields, temperature, and salinity data. The fCO_2 characteristics of the main surface currents (NBC, SEC, NECC, and NEC) are identified, as well as the impact of their seasonal variations on the fCO_2 distribution. Precipitation data are used to determine the ITCZ position. Using empirical relationships between fCO_2 and temperature and salinity, two seasonal maps of the air-sea CO_2 flux are produced from temperature and salinity fields. The trend of seawater fCO_2 over time is examined in a small area, 1°S–1°N and 32°W–28°W, using available cruises. The seawater fCO_2 increased at a lower rate than atmospheric fCO_2 in February-March whereas seawater fCO_2 has increased at the same rate as the atmospheric fCO_2, in October-November.

2. Data and Methods

The PIRATA BR XI cruise departed from Fortaleza on the 20th of March 2009 following a route along 38°W to reach 15°N where the PIRATA mooring was serviced. Then, the ship went back to Natal on the 3rd of April 2009,

Table 1. Cruise Dates, Track, and Vessel Name

Dates	Track	Vessel
	March–April 2009	
3–6 Mar 2009	6°S–15°N	*Monte Olivia*
7–9 Mar 2009	Kourou–15°N	*MN Colibri*
20 Mar 2009 to 3 Apr 2009	Fortaleza-Natal	*N.Oc. Antares*
14–17 Apr 2009	6°S–15°N	*Monte Olivia*
	July–August 2010	
23 Jul 2010 to 6 Aug 2010	Fortaleza-Fortaleza	*N.Oc. Antares*
15–29 Jul 2010	15°N–6°S	*Rio Blanco*
6–8 Aug 2010	15°N–7°N	*MN Colibri*
15–18 Aug 2010	6°S–15°N	*Rio Blanco*

after servicing the PIRATA moorings along 38°W (12°N, 8°N, and 4°N) and the mooring at 0, 35°W. The PIRATA BR XII cruise departed from Fortaleza on the 23rd of July 2010 following a route along 38°W to reach 15°N and went back to Fortaleza on the 6th of August. The servicing sequence of the moorings was 12°N, 15°N, 8°N, and 4°N. At each servicing procedure the ship track was interrupted by around 20 h that might cause discontinuity on the data if the site has strong dynamics.

Underway fCO_2 was measured using an automated system with an infrared analyzer (Licor 7000) described by Lefèvre [2009]. The system was connected to the seawater supply of the ship. A Seabird SBE 21 thermosalinograph was also connected to the same seawater system for recording temperature and salinity underway.

Surface seawater samples for dissolved inorganic carbon (DIC) and total alkalinity (TA) analyses were taken during the cruise and were measured by potentiometric titration using a closed cell, following the method of *Edmond* [1970]. The equivalent points were calculated using the code published by *DOE* [1994]. Certified Reference Material (CRM), supplied by Prof. A. Dickson (Scripps Institutions of Oceanography, San Diego, USA), were used for calibration. The accuracy was estimated at ± 3 μmol/kg for both DIC and TA.

The PIRATA cruises were completed with the underway fCO_2 collected by two ships of opportunity sailing west and east of the PIRATA cruise track using an automated fCO_2 instrument similar to the one described by *Pierrot et al*. [2009]. Since 2006, the merchant ship *MN Colibri*, sailing from Le Havre (France) to Kourou (French Guiana), sampled west of the 38°W section whereas the *Monte Olivia* (and from 2010 the *Rio Blanco*) sailing from Le Havre (France) to Santos (Brazil) sampled further east since 2008. Underway temperature and salinity were recorded on these ships as they were both equipped with a thermosalinograph Seabird SBE 21. In this work, we use only the voyages of the two merchant ships corresponding to the dates of the PIRATA cruises (Table 1), and we focus on the region of the western tropical Atlantic bounded by 6°S–15°N, 55°W–25°W.

The CO_2 flux was calculated as follows:

$$F = k\ K_0 (fCO_{2sw} - fCO_{2atm}) \quad (1)$$

where fCO_{2atm} is the atmospheric fCO_2, fCO_{2sw} is the oceanic fCO_2, k is the exchange coefficient calculated using the formula of *Sweeney et al*. [2007] and the European Centre for Medium-Range Weather Forecasts (ECMWF) wind field, and K_0 is the solubility of CO_2 in seawater taken from *Weiss* [1974].

In order to calculate the trend of atmospheric fCO_2 from 1987 to 2011, we used the monthly molar fraction of CO_2 (xCO_{2atm}) recorded at the atmospheric station at Ragged Point Barbados (13.17°N, 59.43°W) of the NOAA/ESRL Global Monitoring Division (http://www.esrl.noaa.gov/gmd/ccgg/iadv/), and the monthly SST and atmospheric pressure of the NCEP/NCAR (National Centers for Environmental Prediction/National Center for Atmospheric Research) reanalysis project.

For the basin-scale surface circulation, we used a combination of drifter data from the Surface Velocity Program (SVP) with satellite-altimeter data from CNES/Aviso (Archiving, Validation, and Interpretation of Satellite Oceanographic data) [*Niiler et al*., 2003]. The data represent the Ekman-removed ocean circulation at 15 m depth. Detailed explanation about total and Ekman-removed circulation is given by *Lumpkin and Garzoli* [2005], and the data synthesis is described by *Lumpkin and Garzoli* [2011]. Here 19 years (1992 to 2010) of 15 m depth ocean velocity data were used to compute the monthly climatology and seasonal maps, December-January-February (DJF), March-April-May (MMA), June-July-August (JJA), and September-October-November (SON).

Daily products of sea surface temperature TRMM (tropical Rainfall Measuring Mission) Microwave Imager (TMI) imagery were used to obtain monthly maps of SST for the western tropical Atlantic.

Table 2. Sea Surface Salinity (SSS) Root Mean Square Error (RMSE) and Mean Bias Error (MBE) Between Observed and Mercator and Observed and SMOS

	RMSE Mercator	MBE Mercator	RMSE SMOS	MBE SMOS
Colibri	0.49	−0.29	0.49	0.17
Rio Blanco	0.44	−0.01	0.49	0.25
Pirata BR XI 1	0.29	0.04	0.59	0.35
Pirata BR XI 2	0.33	−0.03	0.47	0.22

To estimate the ITCZ position, daily data sets (resolution 2.5°) from the Global Precipitation Climatology Project (GPCP) [*Adler et al*., 2003; *Xie et al*., 2003] were used. Downloaded data were from the website: http://precip.gsfc.nasa.gov/.

Surface salinity fields were obtained from Mercator-Ocean on a 1/4° grid using the system PSY3V3R1 (www.mercator-ocean.fr). In addition, as the salinity data from the SMOS (Soil Moisture and Ocean Salinity) mission were available for the year 2010, the monthly SSS field of July 2010 at 0.25° resolution was also used. The salinities from Mercator and SMOS were collocated to the ship position to compare to the observations made during the three cruises of July 2010. The root mean square error (RMSE) and the mean bias error (MBE) are reported in Table 2. Some differences were expected as Mercator and SMOS salinities are monthly fields and the region is very dynamic. Between 6°S and 15°N, the standard deviation of salinity is 2 for the *Colibri* cruise and range from 0.43 to 0.60 for the cruises further east. Although the RMSE are similar using Mercator or SMOS salinity, and are within the range of observed variability, the SMOS salinity is slightly biased toward higher values with the MBE being greater than 0.17.

3. Surface Circulation and Distribution of fCO_2, SST, and SSS

3.1. Climatology (1992–2010) of Surface Circulation

The climatology (1992–2010) of the surface circulation in the western tropical Atlantic Ocean was computed from the SVP data [*Lumpkin and Garzoli*, 2011], and is presented in Figure 1. A dynamically complex system of currents flows mainly in the zonal direction [*Lumpkin and Garzoli*, 2005; *Stramma and Schott*, 1999]. The westward North and South Equatorial Currents (NEC and SEC)—the equatorward arms of the subtropical gyres—are separated by the eastward North Equatorial Countercurrent (gray shade in Figure 1). This current is composed by a main southern core (sNECC) and a northern branch (nNECC) that lies closer or apart each other along the year [*Stramma et al*., 2005; *Urbano et al*., 2006, 2008]. These eastward branches are mostly driven by the wind field over the whole tropical basin. They are fed predominantly by the North Brazil Current (NBC) [*Schott et al*., 1998] but also receive water from the Amazon Plume and from the NEC. The NECC is the major component of the zonal current system and plays an important role in modulating the heat flux in the tropical Atlantic [*Philander and Pacanowski*, 1986]. The NECC intensifies during summer and fall (Figures 1c and 1d). The NBC is a strong current flowing northwestward along the South American coast and originates from the North Brazil Undercurrent (NBUC), from a northward coastal flow between 10°S and 5°S [*Schott et al*., 1995; *Silveira et al*., 1994], and from waters carried by the surface-intensified South Equatorial Current [*Peterson and Stramma*, 1990]. The NBC retroflection [*Didden and Schott*, 1993; *Wilson et al*., 2002], a result of the vorticity balance, is shown in Figure 1 as the clockwise gyre centered at 5°N, 45°W, at all seasons. The retroflection appears weaker in spring (MAM; Figure 1b) and stronger in fall (SON; Figure 1d). Part of the Amazon River discharge is carried by the retroflection and part of it flows into the Caribbean Sea.

3.2. Surface Distribution in the Western Basin

Figures 2–4 present the distribution of surface velocity (both climatology and observed velocity fields), fCO_2, SST, and SSS west of 38°W, centered at 38°W, and east of 38°W, during early spring 2009 (March/March-April) and late summer 2010 (July-August/August). The velocity data are interpolated to the ship tracks and are plotted as a function of latitude for comparison with fCO_2, SST, and SSS.

The ranges of fCO_2, SST, and SSS are indicated in Table 3. The lowest salinity and fCO_2 values are observed during the western cruises and are explained by the influence of Amazon waters. The highest salinities (>37) are found in the NEC during the Colibri cruises. The maximum fCO_2 is in summer and the minimum SST is in spring (March–April 2009 in Table 3), both in the NEC.

Along the westernmost ship track, in March-April, both climatological and observed velocity fields show a strong separation between the NBC and the NECC (Figure 2a). The two current systems are also associated with different physical and biogeochemical properties (Figures 2b and 2c). The lowest fCO_2 are encountered

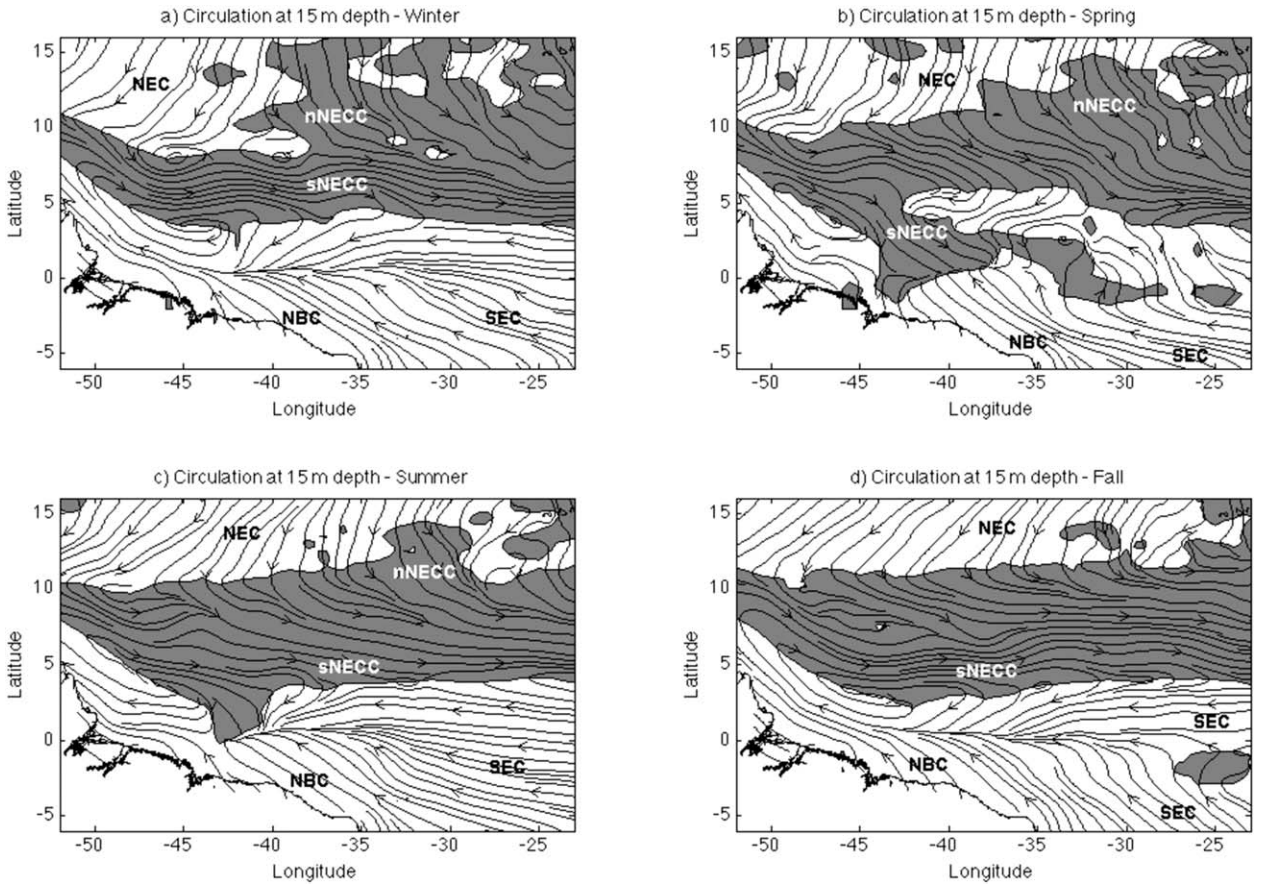

Figure 1. Climatological (1992–2010) maps of 15 m deep ocean velocity data for (a) boreal winter (December-January-February), (b) Spring (March-April-May), (c) Summer (June-July-August), and (d) fall (September-October-November). NEC is the North Equatorial Current, NECC the North Equatorial Countercurrent with nNECC being the northern branch and sNECC the southern branch, NBC the North Brazil Current, and SEC the South Equatorial Current.

in the NBC (Figure 2b). Very low fCO_2 (<270 μatm), low salinity (<34), and temperature higher than 27°C are found near the South American coast in March (spring; Figure 2b) and are caused by the Amazon outflow. At about 7°N, there is a peak of high fCO_2 associated with the NECC and salinity values higher than 36 (Figures 2b and 2c). This salinity signature suggests that the water is from the southern hemisphere brought by the NBC and not by the SEC from the center of the basin as the SEC has low salinity due to the presence of the ITCZ.

In August (summer; Figures 2d–2f), the climatological and observed velocity fields are similar but the observed NEC has small positive velocities suggesting that some eddies are sampled during the cruise (Figures 2d and 2e). Low fCO_2 (close to 7.5°N) and low salinity with temperatures higher than 29°C are observed up to 8°N (Figures 2e and 2f). This water is from the Amazon plume, which joins the northwestward NBC (5°N), retroflects, and feeds the eastward meandering NECC (7°N). Further east, the fCO_2 is higher as dilution with ocean waters occurs during the eastward propagation. The NECC transports little Amazon water during March (spring; Figure 2b) while during August (summer; Figure 2e) it carries most of waters with fCO_2 lower than 370 μatm, low salinity and temperature higher than 29°C (Amazon water). In the region from 12°N to 20°N, the fCO_2 was almost constant around 370 μatm, close to the atmospheric value (Figure 2e). At 11°N, a peak of salinity higher than 36 (Figure 2f) and a peak of fCO_2 are associated with a westward flow.

3.3. Surface Distribution in the Central Basin

At 38°W (Figure 3), the zonal current system appears more evident than in the west. The water comes from the northern and from the southern hemispheres, to meet and mix in the latitudinal band centered at 5°N. In March-April (from here on referred as only March), the two branches of the NECC are clearly identified

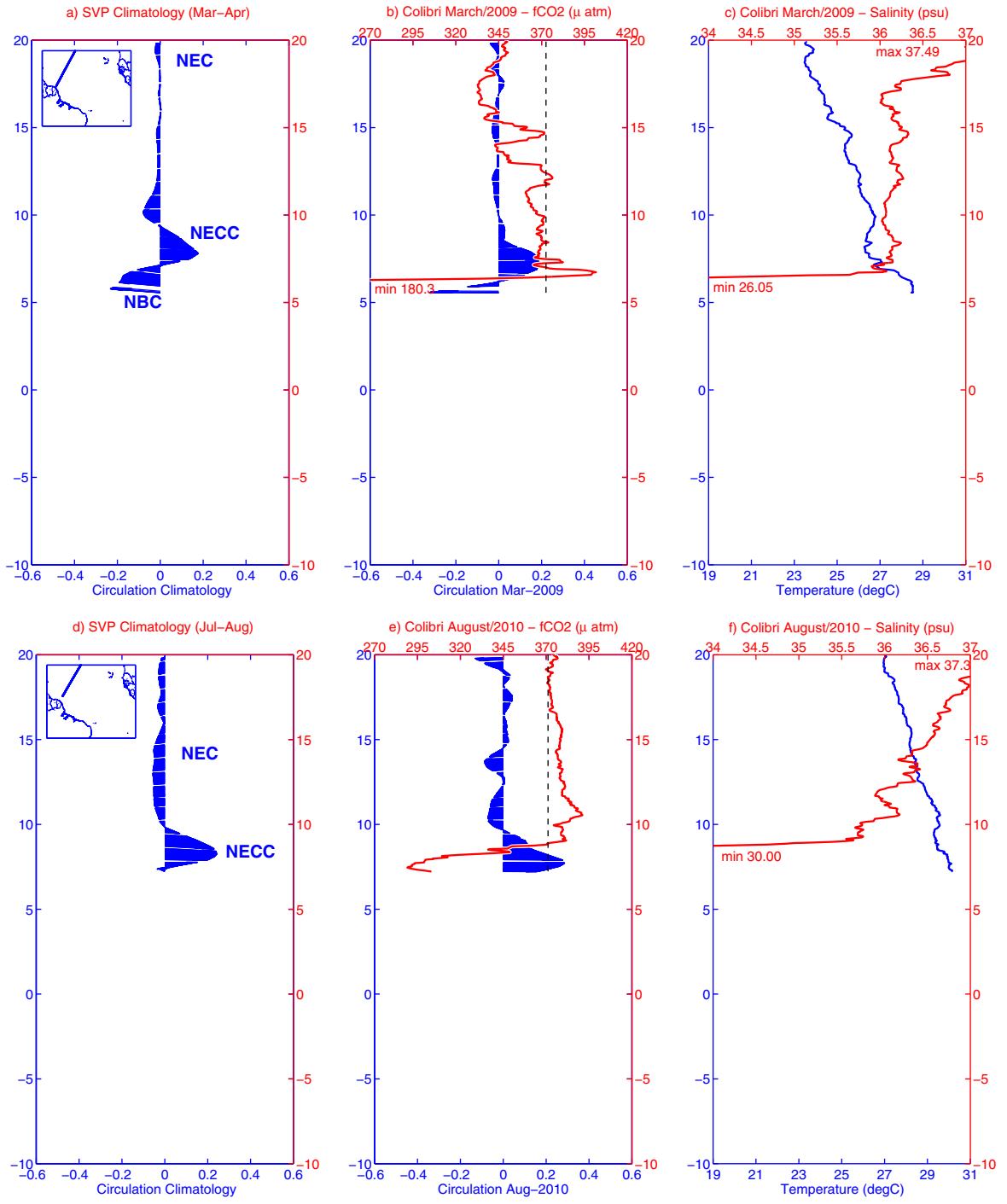

Figure 2. (a) Surface velocity (m/s) from the climatology for March-April along the track of the *MN Colibri* (insert map), (b) latitudinal distribution of surface velocity and seawater fCO_2 (in μatm) with mean atmospheric value of fCO_2 (dashed line) during the voyage of the *MN Colibri* in March 2009, (c) latitudinal distribution of sea surface temperature and sea surface salinity for March 2009, (d) surface velocity (m/s) from the climatology for July-August along the track of the *MN Colibri*, (e) latitudinal distribution of surface velocity and seawater fCO_2 (in μatm) with mean atmospheric value of fCO_2 (dashed line) during the voyage of the *MN Colibri* in August 2010, and (f) latitudinal distribution of sea surface temperature and sea surface salinity for August 2010. The surface currents are the northern North Equatorial Countercurrent (nNECC) and the North Brazil Current (NBC).

(Figure 3a) and the sNECC is more developed during the cruise compared to the climatology (Figure 3b). Water coming from the north has lower fCO_2 and lower SST (winter influence in the northern hemisphere) while water from the south has higher fCO_2 and higher SST (summer influence in the southern hemisphere), which is consistent with seasonal variability (Figures 3b and 3c). In the meeting zone around 5°N, many eddies are contributing to the mixing. At this time of the year, the zonal currents are not strong and the

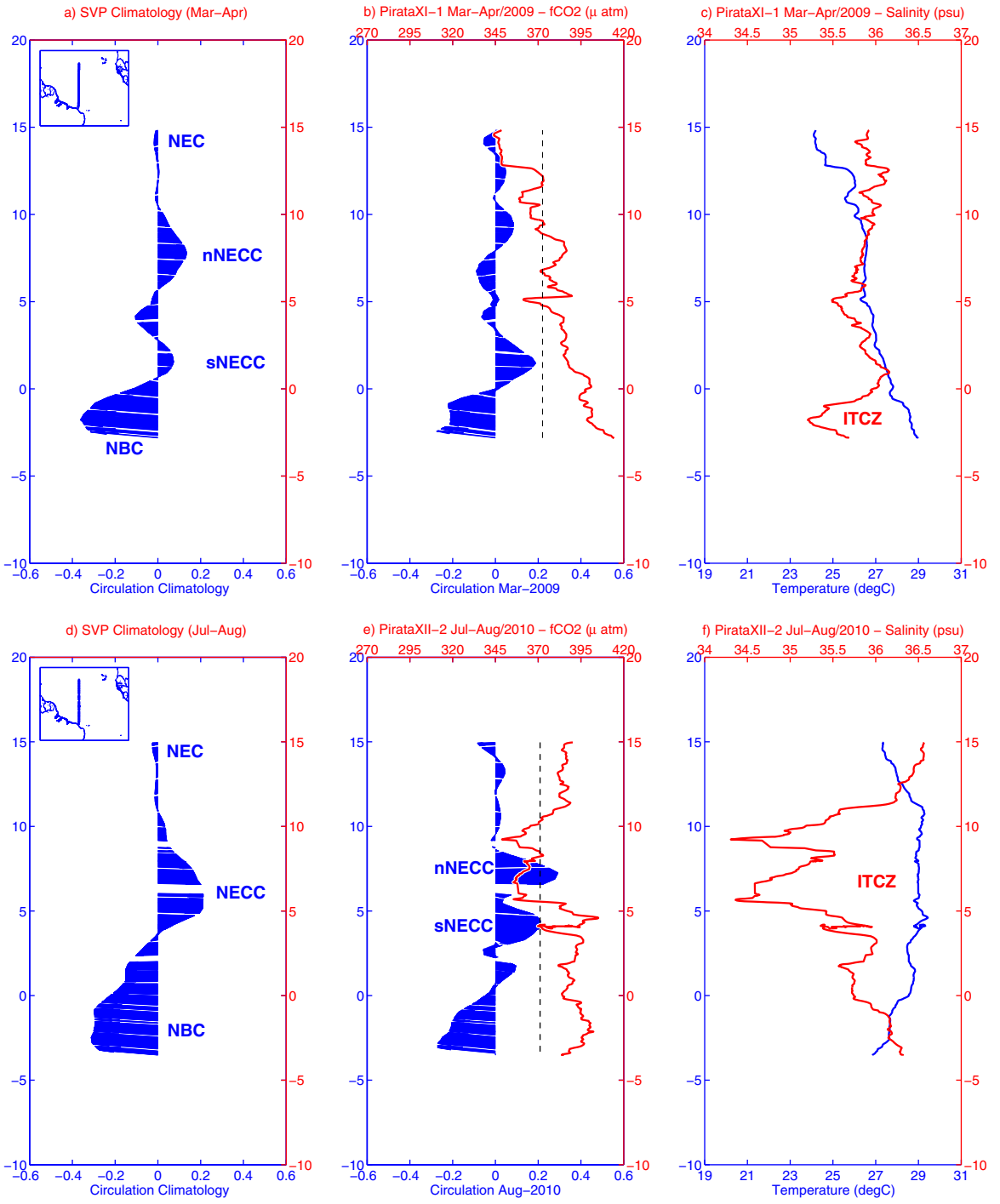

Figure 3. (a) Surface velocity (m/s) from the climatology for March-April along 38°W (insert map), (b) latitudinal distribution of surface velocity and seawater fCO_2 (in μatm) with mean atmospheric value of fCO_2 (dashed line) during the PIRATA cruise in March–April 2009, (c) latitudinal distribution of sea surface temperature and sea surface salinity in March–April 2009, (d) surface velocity (m/s) from the climatology for July-August along 38°W, (e) latitudinal distribution of surface velocity and seawater fCO_2 (in μatm) with mean atmospheric value of fCO_2 (dashed line) during the PIRATA cruise in July–August 2010, and (f) latitudinal distribution of sea surface temperature and sea surface salinity in July–August 2010. NEC is the North Equatorial Current, nNECC is the northern branch of the NECC and sNECC is the southern branch.

ITCZ is located southward (centered at 2°S) as shown by the lower salinity (Figure 3c). From the south up to the equator, water with low salinity (<35.5) and high SST (> 27°) associated with the ITCZ, is transported northwestward by the NBC. This water has also the highest values of fCO_2 along the ship track, being over 395 μatm (Figure 3b). The NECC is a broad band at this time of the year and carries mixed water from the

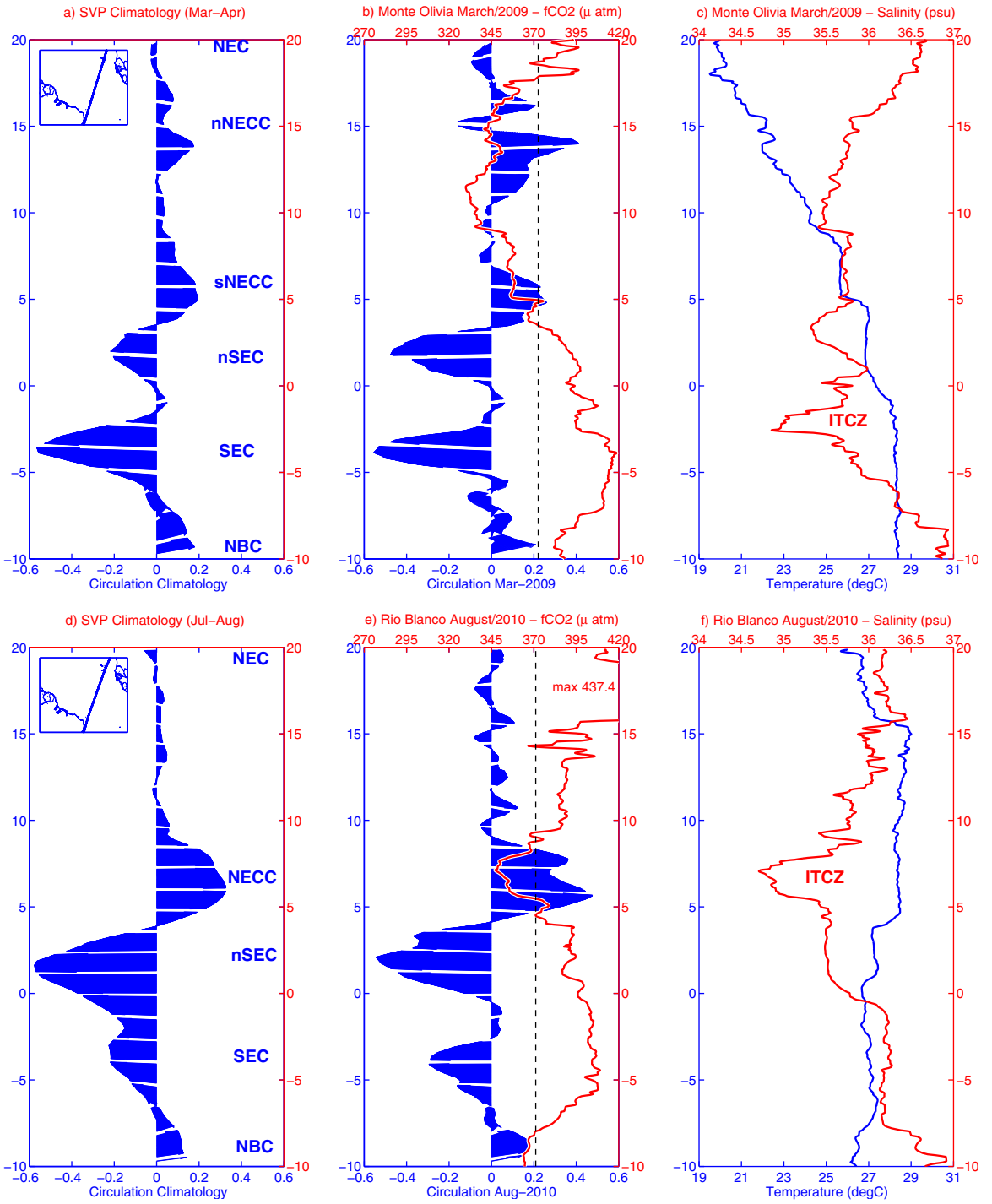

Figure 4. (a) Surface velocity (m/s) from the climatology for March-April along the track of the *Monte Olivia* (insert map), (b) latitudinal distribution of surface velocity and seawater fCO_2 (in μatm) with mean atmospheric value of fCO_2 (dashed line) during the voyage of the *Monte Olivia* in March–April 2009, (c) latitudinal distribution of sea surface temperature and sea surface salinity in March 2009, (d) surface velocity (m/s) from the climatology for July-August along the track of the *Rio Blanco* (insert map), (e) latitudinal distribution of surface velocity and seawater fCO_2 (in μatm) with mean atmospheric value of fCO_2 (dashed line) during the voyage of the *Rio Blanco* in July–August 2010, and (f) latitudinal distribution of sea surface temperature and sea surface salinity in July–August 2010. SEC is the South Equatorial Current with nSEC its northern branch.

NBC retroflection as well as water from the north (coming from the NEC). At 5°N, water from the Amazon mouth, with low fCO_2 and low salinity, identified on the westernmost cruises (Figure 2), is advected westward. An increase of fCO_2 is found between 11°N and 13°N with values around 370 μatm (Figure 3b). This

Table 3. Minimum and Maximum Values of SST (in °C), SSS, and fCO_2 (in μatm) Encountered During the Cruises From 10°S to 20°N

	SST_{min}	SST_{max}	SSS_{min}	SSS_{max}	$fCO_{2\ min}$	$fCO_{2\ max}$
			March–April 2009			
PIRATA, BR XI, leg 1	24.10	28.98	35.09	36.18	343.5	414.5
PIRATABR XI leg 2	24.14	29.60	34.85	36.30	346.4	426.1
Colibri	23.47	28.85	26.05	37.49	180.3	406.9
Monte Olivia, Mar	19.46	28.51	34.65	37.00	329.6	420.4
Monte Olivia, Apr	20.92	29.46	34.98	37.02	348.0	413.2
			July–August 2010			
PIRATA BR XII, leg 1	27.15	29.92	34.48	36.58	347.7	411.1
PIRATA, BR XII, leg 2	26.84	29.52	34.04	36.57	343.1	410.7
Colibri	26.93	30.17	30.00	37.30	288.3	392.1
Rio Blanco, Jul	24.36	29.87	34.78	37.01	359.1	409.7
Rio Blanco, Aug	25.61	29.06	34.69	36.95	346.7	437.4

water is associated with high salinity. Although this water mass is relatively warm (>26°C), this high salinity is found only north of 15°N (Figure 4c). North of 12°N–13°N, a front is observed with lower fCO_2 associated with lower temperature and salinity and the surface current is westward, associated with the NEC (Figures 3b and 3c).

During July-August (from now on referred as August), the zonal currents are more developed and the two branches of the NECC appear as a broad branch on the climatology (Figure 3d). During the cruise, the two branches can be identified with different fCO_2 (Figure 3e). Low fCO_2 was observed between 5.5°N and 10°N surrounded by waters with high fCO_2 to the north and to the south (Figure 3e). The ITCZ at this time of the year lies between 4°N and 12°N according to the data of the Global Precipitation Climatology Project (not shown). Two peaks of low salinity are associated with two minima of fCO_2 (Figures 3e and 3f). The NECC southern branch (south of 5.5°N) transports water mainly from the NBC while the NECC northern branch (north of 5.5°N) carries mixed water, blended of north (from the NEC) and south hemispheric waters. During this season, no north-south gradient of fCO_2 is observed. The fCO_2 is above 380 μatm south of 5°N and north of 10°N (source of CO_2 to the atmosphere) and fCO_2 lower than the atmospheric value (CO_2 sink) are observed near 6°N–10°N where salinity decreases due to the presence of the ITCZ (Figure 3f).

3.4. Surface Distribution in the Eastern Basin

Figure 4 shows the easternmost ship tracks and the corresponding circulation. The locations of the climatological currents (Figure 4a) are similar to those observed during the cruise (Figure 4b). The intensities of the currents show some differences with the observed field exhibiting small-scale variability with small velocities of opposite sign. During March (early spring), the extreme north of the ship track shows fCO_2 between 370 and 400 μatm (Figure 4b) associated with very high salinity (>36.3 psu) and low temperatures (<21°C), which is typical of the water from the northern hemisphere (Figure 4c). Water with low fCO_2, mostly brought from the north by the ocean circulation, occupies the region from 9°N to 17°N (Figure 4b). From 5°N to 9°N, there is mixed water usually transported by the NECC, and with constant values of fCO_2 (∼350 μatm), of temperature (∼26°C), and salinity (∼35.75).

At 2°S–3°S there is a minimum of salinity (<35) associated with a decrease of fCO_2, which coincides with the ITCZ position, located in the SEC at this time of the year. Low salinity and low fCO_2 water appears again at 4°N in the northern branch of the SEC. The extreme south of the ship track shows fCO_2 of 380 μatm (Figure 4b) associated with high salinity and high temperature (Figure 4c) being transported by the NBC close to the coast.

In August (late summer), the NECC and the SEC are more developed both in the climatology (Figure 4d) and during the cruise (Figure 4e). The lowest fCO_2 is restricted to a narrow band from 5°N to 7°N, in the NECC (Figure 4e), due to the presence of the ITCZ characterized by the lowest salinity (Figure 4f). Between 4°S and 4°N, fCO_2 higher than 395 μatm is associated to the SEC branches. The southern SEC branch is saltier and has slightly higher fCO_2 than its northern branch. In the extreme south of the track, the NBC is associated with very high salinity and relatively low fCO_2 (370 μatm). In the northeastern tropical Atlantic, very high fCO_2 (>420 μatm) are found north of 16°N, northwest of the Cape Verde Islands. North of 15°N, in August (late summer), temperatures are over 27°C and salinities over 36.5 (Figure 4f) whereas the ocean is colder and fresher in March (early spring) with temperatures from 24°C to 27°C and salinities from 36 to 36.5 at 16°N (Figure 4c).

4. Drivers of fCO_2 Variability

From the western to the eastern cruises, the fCO_2 distribution shows a very high variability with values lower than 280 μatm, close to the French Guiana coast near 5°N–6°N (Figure 2a), to high fCO_2 values reaching 420 μatm in the SEC in March (Figure 4b) and above 420 μatm in the NEC in August (Figure 4e). The description of the fCO_2, SST and SSS distributions with the ocean circulation of the previous section highlighted different features.

The impact of Amazon waters carried by the NBC is evident in the observations collected by the westernmost cruises on board the *MN Colibri* whereas further north, in the NEC, the CO_2 distribution is affected by the SST (Figures 5a and 5b). In March, the waters are CO_2 undersaturated but in August they become slightly supersaturated (Figures 2a and 2b). SST explains more than 75% of the fCO_2 variability between 10°N and 18°N. The increase of fCO_2 with SST is close to the thermodynamic relationship of 4%/°C in March whereas, in August, fCO_2 increases at a slower rate (Figures 5a and 5b).

The PIRATA cruises along 38°W and the voyages of the *Monte Olivia*/*Rio Blanco* (central and eastward ship tracks) show a systematic north-south increase of fCO_2 for both March and August with generally CO_2 undersaturated waters in the northern North Equatorial Countercurrent (nNECC) and CO_2 supersaturated waters in the NBC and SEC (Figures 3 and 4). The persistence of low fCO_2 in the nNECC region is explained by the low salinity associated with the ITCZ position in July-August whereas, in March-April, when the ITCZ is displaced further south, the seasonal cooling of the boreal winter explains the low fCO_2. This was previously noticed on the monthly voyages of the *Monte Olivia* from France to Brazil [*Lefèvre et al*., 2010].

Along the *Monte Olivia*/*Rio Blanco* tracks (easternmost tracks), the seasonal impact clearly appears in the NBC with higher seawater CO_2 in austral summer (March) whereas a slight CO_2 undersaturation associated with cooler surface temperatures is observed in austral winter (Figure 4). In the SEC, seawater fCO_2 is always high and the presence of the ITCZ near 2°S in March leads to a slight decrease of fCO_2 but the water remains supersaturated in CO_2.

The north-south CO_2 gradient, encountered within the SEC and the NECC, corresponds to a different pattern in SST. In March-April, fCO_2 is increasing with SST, in the latitudinal band 6°S–6°N (Figures 5c and 5d). During the *Monte Olivia* voyages (spring) the correlation coefficients between fCO_2 and SST were 0.88 in March and 0.92 in April. In March, it is early springn (still under winter influence) north of the equator and it is early fall south of the equator (still under summer influence). The cooling effect explains the low fCO_2 north of the equator. South of the equator there is heating and high SSTs are associated with high fCO_2. North of the equator the water is colder as it is early spring and fCO_2 is lower than south of the equator where the water is warmer and fCO_2 is higher. The same pattern is observed during the PIRATA cruises along 38°W with a correlation coefficient of 0.89 between fCO_2 and SST in 2009.

In August, along the *Rio Blanco* track (east), even though the SST measured presented higher values north of the equator (5°N–15°N), the highest fCO_2 was found in the southern hemisphere associated with the lowest SST (Figures 4e and 4f). In boreal summer (July-August), fCO_2 is decreasing from 6°S to 6°N with increasing temperature during the PIRATA cruises and the voyages of the *Rio Blanco* (Figures 5e and 5f). The correlation coefficients between fCO_2 and SST are −0.91 in July and −0.89 in August, during the voyages of the *Rio Blanco*. It is also negative during the PIRATA cruise (−0.49). It means that different processes occur between March-April and July-August. In March-April (boreal early spring), the fCO_2 distribution seems to be mainly governed by seasonal variability of SST while in July-August this is not the dominant mode of variability. The high fCO_2 south of the equator in July-August suggests some carbon supply in this region. The source of carbon might come from the equatorial upwelling, as it is more pronounced at this time of the year than in March-April.

The distribution of DIC during the PIRATA cruises shows the impact of the ITCZ. Low values of DIC were found near 2°S in March 2009, and between 5°N–10°N in July 2010 (Figure 6a). In 2009, the mean value of DIC is 2016.0 ± 18.4 μmol/kg whereas in 2010 the variability is much higher (2000.7 ± 32.1 μmol/kg). Much lower DIC concentrations are observed when the ITCZ is in the northern hemisphere. After removing the salinity effect, the distribution of DIC exhibits higher values in the southern hemisphere in the NBC in July 2010 (Figure 6b). This is consistent with some carbon supply from the equatorial upwelling transported by the SEC that feeds the NBC. The surface distribution of alkalinity (Figure 6c) shows the same features as the distribution of the DIC. A pronounced alkalinity decrease is associated with the ITCZ position. However,

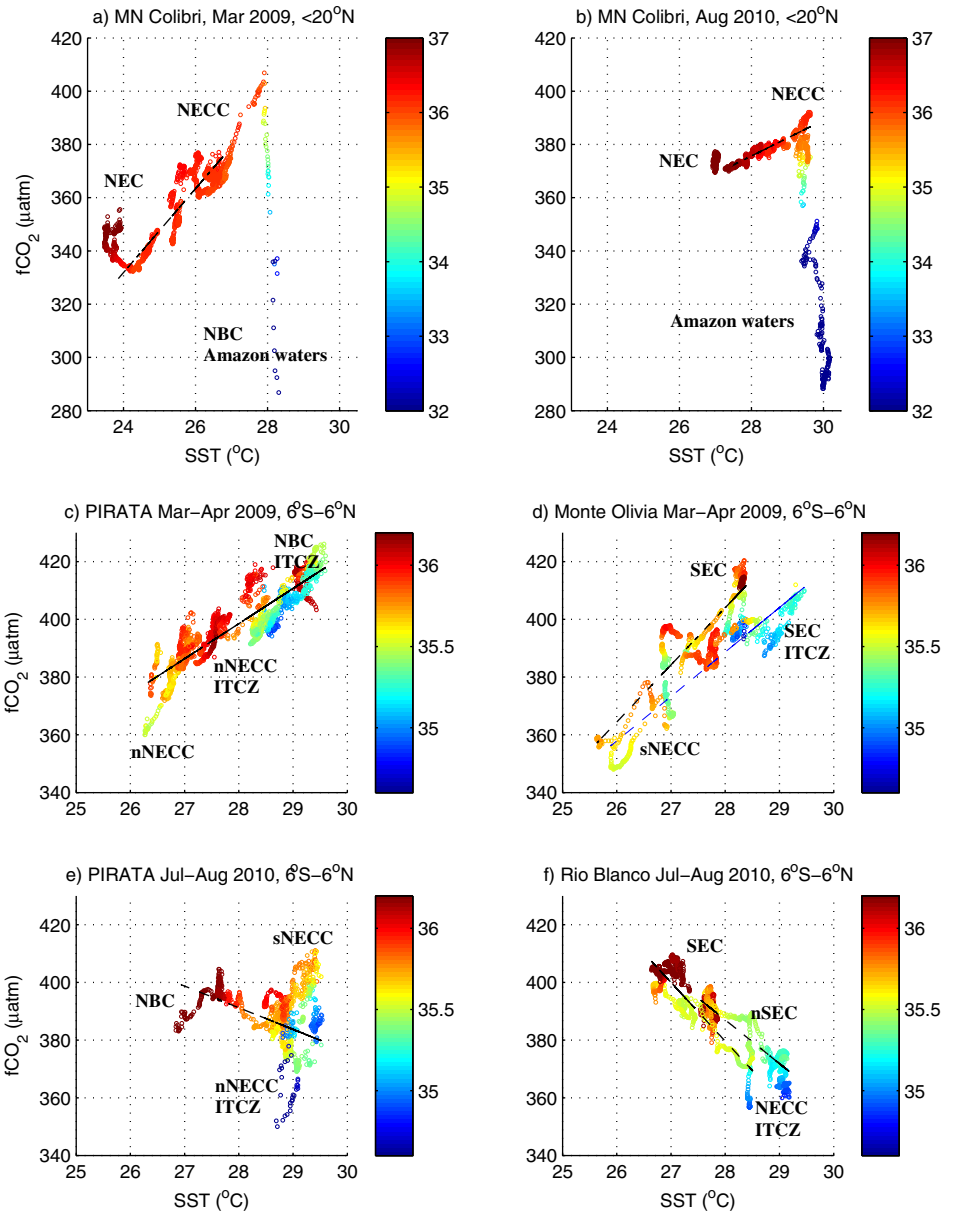

Figure 5. fCO_2 as a function of SST (a) during the voyage of the *MN Colibri* in March 2009 south of 20°N, (b) during the voyage of the *MN Colibri* in August 2010 south of 20°N, (c) during the PIRATA cruise of March–April 2009 between 6°S and 6°N, (d) during the voyages of the *Monte Olivia* in March and April 2009 between 6°S and 6°N, (e) during the PIRATA cruise of July–August 2010 between 6°S and 6°N, and (f) during the voyages of the *Rio Blanco* in July and August 2010 between 6°S and 6°N. Sea surface salinity is color coded. The water masses corresponding to the main systems of currents are indicated.

when alkalinity is normalized by salinity (Figure 6d), alkalinity becomes almost constant (2335.2 ± 4.7 µmol/kg in 2009 and 2333.0 ± 3.2 µmol/kg in 2010). This suggests that evaporation and precipitation are the main factors explaining the variability of alkalinity.

5. Estimate of the Air-Sea CO_2 Flux for the Region 6°S–15°N, 25°W–55°W

5.1. Seasonal Maps

Empirical relationships are useful to reconstruct fCO_2 data and are used to determine trends [e.g., *Lefèvre et al.*, 2004; *Park et al.*, 2010] or to provide an estimate of the flux in a given region. Most of the empirical relationships are mainly expressed as a function of SST.

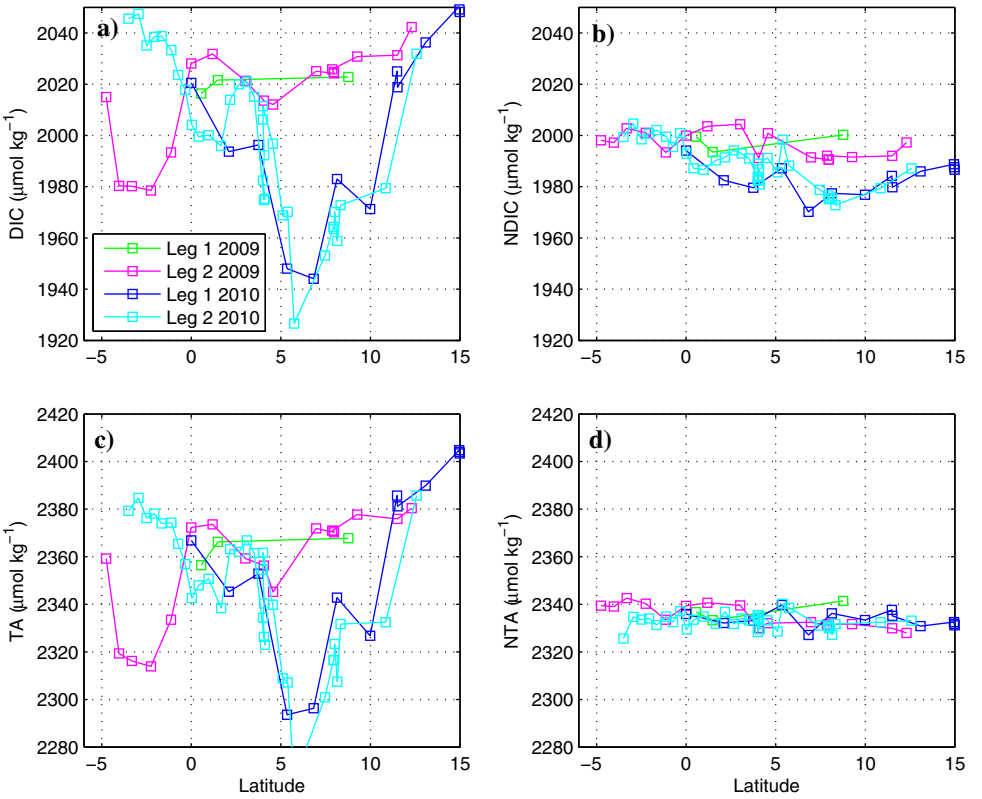

Figure 6. (a) Dissolved inorganic carbon (in μmol kg^{-1}), (b) normalized dissolved inorganic carbon at a salinity of 35.5 (NDIC = DIC * 35.5/salinity), (c) total alkalinity (in μmol kg^{-1}), and (d) normalized total alkalinity at a salinity of 35.5 as a function of latitude during the PIRATA cruises in 2009 and 2010.

In the region 6°S–15°N, 25°W–55°W, fCO_2 is strongly affected by seasonal variations of temperature with decreasing (increasing) fCO_2 associated to winter cooling (summer warming) but also by salinity variations with the seasonal migration of the ITCZ. In addition, river discharge decreases fCO_2 and the equatorial upwelling increases fCO_2 by supplying CO_2-rich waters to the surface. Averaging the data of the three cruises on a 0.5° spatial resolution, a relationship between fCO_2 and temperature and salinity is obtained:

$$\text{For March to April}: \quad fCO_2 = -593.6 + 12.9\ SST + 17.5\ S \tag{2}$$

with an error on the predicted fCO_2 of 10.6 μatm, and a coefficient of determination $r^2 = 0.82$ using 187 data. A regression with SST only would lead to an error on fCO_2 of 20 μatm, and a coefficient of determination $r^2 = 0.36$.

$$\text{For July to August}: \quad fCO_2 = -24.7 - 3.4\ SST + 14.2\ S \tag{3}$$

with an error on the predicted fCO_2 of 9 μatm, and a coefficient of determination $r^2 = 0.75$ using 197 data. A regression with SST only would lead to an error of 15 μatm and a coefficient of determination $r^2 = 0.31$. This highlights the importance of salinity variations in controlling the CO_2 distribution in the tropical Atlantic. For both relationships, the residuals do not show any trend against temperature and salinity.

Determining the fit without averaging the data gives a higher error on fCO_2 (12.5 and 9.7 μatm for March-April and July-August, respectively) and a lower coefficient of determination ($r^2 = 0.75$ and $r^2 = 0.69$ for March-April and July-August, respectively). Averaging the data has the advantage of filtering the small-scale variability. However, there is not a significant improvement of the fit after removing this variability, suggesting that small-scale variability only cannot explain the error on fCO_2.

Table 4. Mean Temperature, Salinity, and fCO_2 for the Different Cruises (in March 2009 and July 2010) and Calculated From the Map in March and July 2010

	Colibri	PIRATA	*Monte/Rio*	Map $< 45^oW$	Map $> 40^oW$
			March, 2.5°N–15°N		
fCO_2	358.9 ± 33.1	374.3 ± 13.0	351.5 ± 14.4	384.2 ± 17.4	384.3 ± 10.1
SST	26.4 ± 0.8	26.3 ± 0.8	24.7 ± 1.6	27.3 ± 0.6	27.08 ± 0.98
S	35.63 ± 1.90	35.89 ± 0.17	35.62 ± 0.14	35.70 ± 1.05	35.88 ± 0.20
			July, 2.5°N–15°N		
fCO_2	366.4 ± 29.4	381.2 ± 11.8	383.4 ± 12.4	368.6 ± 26.4	379.4 ± 10.6
SST	29.14 ± 0.58	28.67 ± 0.72	28.75 ± 0.65	28.95 ± 0.46	28.72 ± 0.71
S	35.03 ± 2.07	35.75 ± 0.60	35.68 ± 0.48	34.83 ± 1.79	35.54 ± 0.60
			March, 6°S–2.5°N		
fCO_2		401.7 ± 9.4	402.7 ± 9.9	366.3 ± 61.8	407.5 ± 7.0
SST		28.2 ± 0.7	27.8 ± 0.6	28.8 ± 0.4	28.77 ± 0.42
S		35.69 ± 0.36	35.68 ± 0.33	20.2 ± 14.8	35.81 ± 1.04
			July, 6°S–2.5°N		
fCO_2		391.1 ± 5.2	386.3 ± 7.8	352.5 ± 54.6	387.7 ± 4.7
SST		28.23 ± 0.74	28.07 ± 0.49	28.93 ± 0.49	27.93 ± 0.57
S		35.69 ± 0.36	35.68 ± 0.33	22.80 ± 14.4	35.80 ± 1.08

The two relationships have a temperature coefficient of opposite sign. In March-April, the positive coefficient suggests that the dominant process is the warming of seawater leading to increasing fCO_2. The temperature coefficient is also close to the 4%/°C increase, which corresponds to the thermodynamic effect. On the contrary, in July-August, the temperature coefficient is negative, which is characteristic of upwelling regions where fCO_2 increases at low temperature because of the supply of CO_2-rich and colder waters to the surface. In July-August, the coefficient of determination is lower than in March-April. This is the time of the year when the equatorial upwelling is stronger. A possible explanation is that in July-August, the upwelling effect is stronger and tends to compensate, or even dominate, over the warming effect.

Monthly SST from TMI and salinity fields from Mercator can be used to map fCO_2 for March 2009, using equation (2) for salinity greater than 15. Salinity lower than 15 would give negative fCO_2. The temperature and salinity fields have been averaged to provide data on a 0.5° latitude × 0.5° longitude grid. Using SST and SSS fields in July 2010, fCO_2 is calculated with equation (3) between 6°S and 15°N, 24°W–50°W for salinity greater than 10. The mean values of temperature, salinity and fCO_2 are compared with the observations (Table 4). West of 45°W, low salinities due to the Amazon discharge explain the large variability in salinity and fCO_2. In July 2010, the mean values are close to the observations made on board the *MN Colibri* between 2.5°N and 15°N.

In the region 6°S–2.5°N, the mean values east of 40°W, far from the coastal influence, compare well with the observations made during the PIRATA (central track) and Monte Olivia/Rio Blanco (eastern track) cruises. The mean values west of 45°W include the lowest salinities located close to the coast and the variability is very high with a standard deviation of 14 for salinity and above 50 μatm for fCO_2.

The mean CO_2 fluxes calculated from the three cruises in March 2009 and July 2010 and from the seasonal maps are given in Table 5 for different latitudinal bands. The area south of 2.5°S, dominated by the NBC and the SEC, is always a strong source of CO_2 for the atmosphere with a flux greater than 3 mmol $m^{-2}d^{-1}$ except for the gridded map in March 2009 which gives a lower CO_2 flux.

The equatorial band 2.5°S–2.5°N is also a source of CO_2 for the atmosphere that is lower than in the band 6°S–2.5°S. North of 2.5°N and south of 8°N, a strong CO_2 sink is observed in March and July during the voyages of the *MN Colibri* as waters from the Amazon plume are located in this region. Further east, given the variability associated with the estimate of the flux, near-equilibrium conditions are observed. Between 8°N and 15°N, a strong CO_2 sink is sampled by the three cruises in March while it turns to a CO_2 source or near-equilibrium conditions in July, which is consistent with the seasonal variations. The cooling of surface water in March leads to an uptake of CO_2 whereas in July the surface warming explains the CO_2 outgassing or neutral conditions (Table 5).

Using equations (2) and (3) for calculating seawater fCO_2, the monthly TMI SST fields of March 2009 and July 2010, the monthly salinity fields from Mercator, the wind fields from ECMWF and the monthly atmospheric value at the Ragged Point Barbados station, a map of the flux of CO_2 can be constructed. At the atmospheric station Ragged Point Barbados, the monthly atmospheric value is 372.6 μatm in March 2009

Table 5. Mean Flux of CO_2 With ± One Standard Deviation (in mmol $m^{-2}d^{-1}$) Calculated Using ECMWF Wind Speeds for the Different Cruises (Voyages of the *MN Colibri* in the West, PIRATA Cruises Along 38°W, and Voyages of the *Monte Olivia* and *Rio Blanco* Further East), Average of the CO_2 Flux of the Three Cruises, and Mean CO_2 Flux Calculated From the Seasonal Maps for March 2009 and July 2010 in Several Latitudinal Bands[a]

Region	*Colibri* (West)	PIRATA (38°W)	*Monte/Rio* (East)	Mean	Grids	Grid SMOS
			March 2009			
6°S–2.5°S		3.43 ± 1.26	3.62 ± 0.96	3.52	2.19 ± 0.85	
2.5°S–2.5°N		1.85 ± 0.41	1.20 ± 0.19	1.52	0.52 ± 3.24	
2.5°N–8°N	−2.27 ± 7.29	1.04 ± 1.16	−0.56 ± 0.75	−0.60	0.20 ± 2.39	
8°N–15°N	−1.40 ± 1.33	−1.73 ± 1.97	−2.42 ± 0.60	−1.85	−2.06 ± 1.96	
			July 2010			
6°S–2.5°S		4.42 ± 1.51	3.37 ± 0.67	3.89	3.71 ± 0.58	3.69 ± 1.06
2.5°S–2.5°N		3.30 ± 1.53	1.92 ± 1.24	2.61	2.06 ± 3.20	3.06 ± 1.37
2.5°N–8°N	−2.89 ± 0.31	0.49 ± 0.60	0.09 ± 0.17	−0.77	−0.08 ± 1.23	0.07 ± 0.90
8°N–15°N	0.16 ± 0.50	1.34 ± 1.12	0.27 ± 0.34	0.59	1.49 ± 1.45	2.11 ± 1.81

[a]The last column corresponds to the CO_2 flux estimated using the SMOS data.

and 371.1 μatm in July 2010. For comparison, the mean atmospheric fCO_2 measured during the PIRATA cruise was 371.4 ± 3.0 μatm in 2009 and 369.7 ± 3.0 μatm in 2010.

The maps reproduce the patterns observed on the individual cruises with sources and sinks observed at the same location (Figure 7).

The strongest source of CO_2 occurs south of 2.5°S in the SEC that is influenced by the upwelling of CO_2-rich waters. In the equatorial region, a source of CO_2 is also observed but it is much stronger in July than in March. Higher SST, SSS, and winds can explain this difference as the seawater fCO_2 values are very close. In the region 2.5°N–8°N, the CO_2 flux in July is slightly negative. The presence of the ITCZ is visible with low CO_2 flux in the NECC region across the basin in July. However, this feature is not visible on the map using the SMOS salinity because of the bias toward higher salinity. North of 8°N, the region is a sink of CO_2 in winter, with waters colder by more than 4°C compared to July, and low seawater fCO_2.

It is difficult to compare the mean CO_2 flux obtained by the individual cruises with the gridded maps because of the very high standard deviation (Table 5) as a consequence of the high variability of the region. In particular, the Colibri cruises are affected by the Amazon outflow in the region 2.5°N–8°N. However, the main features are present in the maps, such as the stronger outgassing south of the equator at both seasons and the cooling (warming) north of 8°N in March (July) leading to a CO_2 sink (source). On average, the CO_2 flux is −0.40 ± 2.77 mmol $m^{-2}d^{-1}$ in March 2009 and 1.32 ± 2.18 mmol $m^{-2}d^{-1}$ in July 2010. The cooling effect in March is dominating the region and explains the resulting CO_2 uptake. The high standard deviation associated with the mean flux highlights the high variability observed in this region, an important contributor being the Amazon plume.

5.2. Evolution of the Source of CO_2 Over Time

Our estimate of ΔfCO_2 is −1.82 ± 23.9 μatm in March 2009 in the region 6°S–15°N, 52°W–24°W. For the month of March, the climatology of *Takahashi et al*. [2009], made for the reference year 2000, gives an estimate of 12.1 ± 17.9 μatm in this region, which corresponds to averaging 20 pixels. In July 2010, ΔfCO_2 is −9.22 ± 16.4 μatm compared to the climatological value for July of 17.3 ± 8.7 μatm. This would suggest that seawater fCO_2 did not increase of the same rate as atmospheric CO_2 but at a slower rate, i.e., ΔfCO_2 is decreasing over time instead of being constant. However, due to the high variability it is difficult to conclude on any trend. The strong influence of dynamical processes on water properties and the scarce fCO_2 data in the tropical Atlantic make difficult the detection of trends on fCO_2.

As *Park and Wanninkhof* [2012] found a decreasing trend, further north, in the tropical Atlantic on a small area 19°N–20°N, 65°W–68°W, we investigated the CO_2 trends in the SEC in the small area 1°S–1°N, 32°W–28°W. In order to avoid any bias due to the seasonal variability, we consider the cruises made in February-March and October-November, where the number of cruises is the highest. The available cruises range from 1983 to 2011 in February-March and from 1991 to 2010 in October-November (Table 6).

In February-March, the increase of seawater fCO_2 is slower than in October-November with a rate of increase of 1.06 ± 0.13 μatm/yr (coefficient of determination r^2 of 0.93) compared to 1.64 ± 0.21 μatm/yr

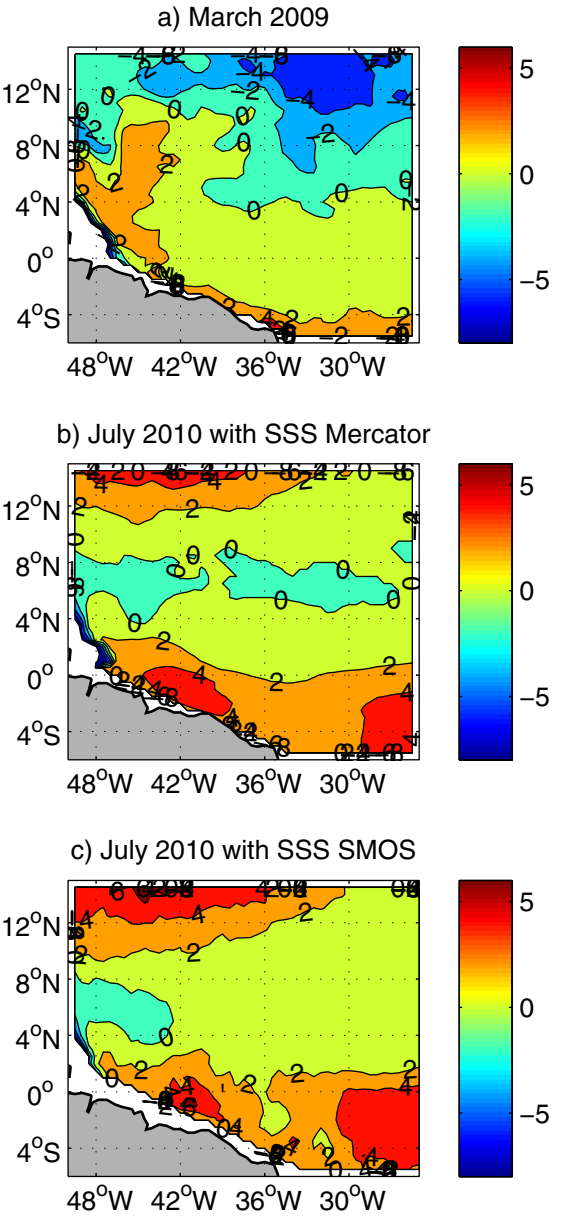

Figure 7. Map of the CO_2 flux (a) in March 2009, (b) in July 2010 with salinity from Mercator, and (c) in July 2010 with salinity from SMOS.

with $r^2 = 0.89$ (Figure 8a). However, the comparison of the slopes using a Student *t* test does not confirm that the slopes are significantly different. When the year 1983 is excluded from the oceanic data, the seawater fCO_2 increases at a rate of 0.88 ± 0.23 μatm/yr. In that case, the rates of increase in the atmospheric and oceanic fCO_2 were significantly different ($p < 0.001$).

The atmospheric trend of fCO_2 is determined at Ragged Point Barbados. Atmospheric fCO_2 measured during the cruises are in agreement with the fCO_2 at the atmospheric station. There is no significant difference in the atmospheric trends between the two periods of time with an increase of 1.66 ± 0.03 μatm/yr in February-March compared to 1.63 ± 0.03 μatm/yr in October-November (Figure 8b).

In February to March, the atmospheric fCO_2 increased at a higher rate than the oceanic fCO_2 whereas, in October-November, atmospheric and oceanic fCO_2 increased at about the same rate. For both periods, a slight increase of sea surface temperature was observed. In October-November, the SST increased by 0.06 ± 0.02°C/yr ($r^2 = 0.54$) and in February-March no trend was distinguishable with a variation of 0.022 ± 0.022°C/yr ($r^2 = 0.16$). Using the SST Reynolds led to a slight increase of SST for both periods with values of 0.03 ± 0.01°C/yr ($r^2 = 0.16$) in October-November, and 0.009 ± 0.005°C/yr ($r^2 = 0.05$) in February-March. Therefore, the oceanic CO_2 increase was not caused solely by the warming of surface waters. The observed CO_2 trends could be explained by anthropogenic CO_2 uptake.

In February-March, the slower oceanic increase compared to the atmospheric increase suggests that the findings of *Park and Wanninkhof* [2012] might also be valid south of their region of study. Also, this would confirm the results of *Goyet et al.* [1998] who found a decreasing source of CO_2 in the tropical Atlantic when comparing the WOCE A15 data with the FOCAL data. The analysis of *McKinley et al.* [2011] suggests an indistinguishable trend for the subtropical permanently stratified biome from 1987 to 2009 but a slower increase of seawater fCO_2 from 1983 to 2009. In October-November, our results show an ocean CO_2 increase similar to the atmospheric increase but the error on the slope of the regression is quite large. Nevertheless, a different oceanic CO_2 increase rate in this region could be explained by the equatorial dynamics. In October-November, the vertical stratification is stronger than in February-March [*Emery et al.*, 1984] so the surface

Table 6. List of the Cruises in the Regions 1°S–1°N, 32°W–28°W in February to March and October to November

Cruises	Month and Year	Reference
	February–March	
TTO-TAS Leg 3	Feb 1983	*Weiss et al.* [1992]
WOCE A17	Mar 1994	*Rios et al.* [2005]
FICARAM 2	Mar 2001	*Padin et al.* [2009]
TropInt02	Feb 2002	*Wanninkhof et al.* [2008]
Monte Olivia	Feb 2009	*Lefèvre et al.* [2010]
Monte Olivia	Mar 2009	*Lefèvre et al.* [2010]
Rio Blanco	Mar 2011	*Lefèvre et al.* [2013]
	October–November	
OACES Leg 1	Jul 1991	*Wanninkhof and Hendee* [1991]
FICARAM 1	Nov 2000	*Padin et al.* [2009]
FICARAM 3	Nov 2001	*Padin et al.* [2009]
FICARAM 5	Nov 2002	*Padin et al.* [2009]
FICARAM 7	Nov 2004	*Padin et al.* [2009]
FICARAM 10	Nov 2006	*Padin et al.* [2009]
FICARAM 12	Nov 2007	*Padin et al.* [2009]
Monte Olivia	Oct 2008	*Lefèvre et al.* [2010]
Monte Olivia	Nov 2008	*Lefèvre et al.* [2010]
Rio Blanco	Oct 2010	*Lefèvre et al.* [2013]

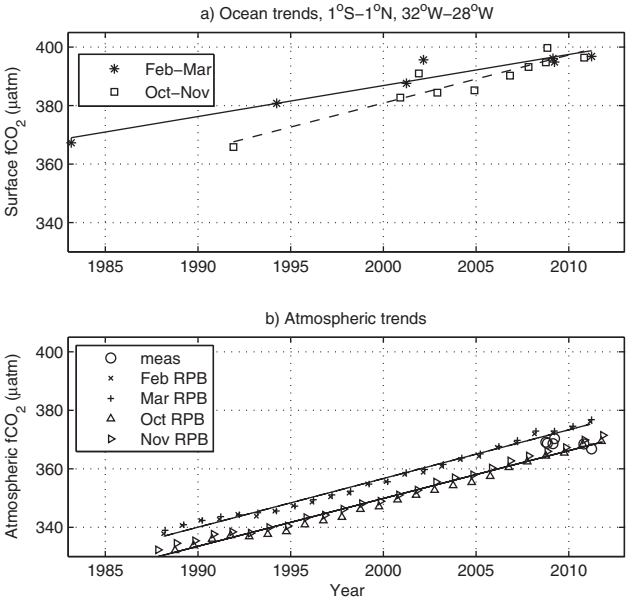

Figure 8. (a) Evolution of seawater fCO_2 over time in the region 1°S–1°N, 32°W–28°W in February-March and October-November using the cruises listed in Table 5. The solid line corresponds to the fit in February-March and the dashed line to the fit in October-November. (b) Evolution of monthly atmospheric fCO_2 over time in the region 1°S–1°N, 32°W–28°W at the atmospheric station Ragged Point Barbados (RPB) and mean atmospheric values obtained during the voyages of the *Monte Olivia* (2008, 2009) and *Rio Blanco* (2010, 2011). The solid lines correspond to the linear regression in February-March and October-November of the atmospheric fCO_2 at Ragged Point Barbados with time.

ocean becomes isolated from the subsurface ocean and tends to equilibrate more quickly with the atmosphere, which would explain a similar increase of fCO_2 in the ocean and the atmosphere. In February-March, the ocean is less stratified and subsurface waters that have not been in contact with the atmosphere for a long time mix with surface waters. This would cause the seawater CO_2 increase to lag behind the atmospheric rate of increase.

As more data are being collected in this region, an analysis of the trend in the western tropical Atlantic will become possible to confirm or deny these results as well as the extension of the area and the cause for this potential decrease of the CO_2 source.

6. Conclusions

The fCO_2 distribution in the western tropical Atlantic was documented in March–April 2009 and July–August 2010 with three cruises almost made in a synoptic way for each period. Close to the American shelf, the North Brazil Current carries Amazon waters when it arrives north of the equator, where the Amazon mouth is located. Along 38°W, the NBC is supersaturated in CO_2 as it is fed by the SEC that carries waters from the equatorial upwelling. South of ~8°S, seasonal variations are responsible for lower fCO_2 in August (austral winter) and higher fCO_2 in March (late austral summer/early austral fall). The SEC and the southern branch of the NECC are supersaturated in CO_2 even when the ITCZ is located south of the equator, near 2°S, in March. Although a decrease of fCO_2 is associated with the ITCZ, the fCO_2 remains above the atmospheric value. Waters of the northern NECC are usually undersaturated in CO_2 due to the Amazon discharge, the presence of the ITCZ in July and the cooling in March (late boreal winter/early boral spring). North of 10°N, the seasonal variations explain the lower fCO_2 values in March compared to the fCO_2 values in August (boreal summer). These features of the fCO_2 distribution, associated with the main current systems, are disturbed by the small-scale variability (vortices), which can induce local decrease or increase of fCO_2.

Acknowledgments
We are very grateful to the Brazilian navy for their help with the CO_2 measurements on board the *R/V Antares*. We thank the Compagnie Maritime Nantaise (MN) and the Hamburg Süd shipping companies for allowing the installation of our CO_2 equipment on board their ships. We are very grateful to the officers and crew of the *MN Colibri*, the *Monte Olivia*, the *Rio Blanco*, and the *N.O. Antea* for their help on board with the measurements. Seawater samples were analyzed for DIC and TA by the SNAPO-CO_2 at LOCEAN. Precipitation data from the Global Precipitation Climatology Project (GPCP) were downloaded from the Giovanni online data system, developed and maintained by the NASA Goddard Earth Sciences (GES) Data and Information Services Center (DISC). We also acknowledge the TRMM mission scientists and associated NASA personnel for production of the data used in this research effort. TMI data are produced by Remote Sensing Systems and sponsored by the NASA Earth Science and REASoN DISCOVER project. They are available at www.remss.com. NCEP reanalysis derived data and NOAA_OI_SST_V2 data were provided by the NOAA/OAR/ESRL PSD, Boulder, Colorado, USA, from their web site at http://www.esrl.noaa.gov/psd/.The SMOS data were obtained from the "Centre Aval de Traitement des Données SMOS" (CATDS), operated for the "Centre National d'Etudes Spatiales" (CNES, France) by IFREMER (Brest, France). We acknowledge support from the PIRATA program, the European Integrated Projects CARBOOCEAN (contract 511176-2) and CARBOCHANGE (grant agreement 264879), the Institut de Recherche pour le Développement (IRD), and the national program LEFE CYBER. The authors are also thankful to Rick Lumpkin from AOML/NOAA, who did the synthesis of, and kindly provided, the near-surface velocity data for the tropical Atlantic. We are grateful to two anonymous reviewers for providing constructive comments on the manuscript.

The fCO_2 is mainly driven by sea surface temperature and salinity variations and strong correlations between fCO_2 and the surface temperature and salinity could be determined. Using the correlations, two seasonal maps of fCO_2 have been obtained in the region 6°S–15°N, 52°W–24°W for March 2009 and July 2010 using temperature and salinity fields. Overall, the temperature variations dominate and explain the sink of CO_2 in March 2009 with a CO_2 flux of -0.40 mmol $m^{-2}d^{-1}$ whereas in July 2010 this region is a source of CO_2 of 1.32 mmol $m^{-2}d^{-1}$.

Comparison of the fCO_2 with the few cruises available in the western equatorial region, in a small area (1°S–1°N; 32°W–28°W), suggests that the source of CO_2 might be decreasing or constant over time. However, the influence of the dynamical processes of the water properties in this region and the poorly known consequences of the physical interannual variability (e.g., El Niño–Southern Oscillation (ENSO) connections, Atlantic ENSO) make difficult the detection of the fCO_2 trend over time and the identification of the causes.

More synoptic cruises or moorings are required to better assess the CO_2 flux throughout the year and its trend over time. Future changes in surface temperature and salinity could affect the source of CO_2. Increasing SST would increase the CO_2 outgassing while high precipitation would decrease it. A change of the equatorial upwelling (e.g., depth of upwelled water) would also affect the CO_2 trends.

References

Adler, R. F., et al. (2003), The version 2 Global Precipitation Climatology Project (GPCP) monthly precipitation analysis (1979-Present), *J. Hydrometeorol.*, *4*, 1147–1167.
Andrié, C., C. Oudot, C. Genthon, and L. Merlivat (1986), CO_2 fluxes in the tropical Atlantic during FOCAL cruises, *J. Geophys. Res.*, *91*(C10), 11,741–11,755.
Bourlès, B., et al. (2008), The PIRATA program: History, accomplishments and future directions, *Bull. Am. Meteorol. Soc.*, *89*, 1111–1125.
Chen, C.-T. A., T.-H. Huang, Y.-H. Fu, Y. Bai, and X. He (2012), Strong sources of CO_2 in upper estuaries become sinks of CO_2 in large river plumes, *Curr. Opin. Environ. Sustainability*, *4*, 179–185.
Cooley, S. R., and P. L. Yager (2006), Physical and biological contributions to the western tropical North Atlantic Ocean carbon sink formed by the Amazon River plume, *J. Geophys. Res.*, *111*, C08018, doi:10.1029/2005JC002954.
Cooley, S. R., V. J. Coles, A. Subramaniam, and P. L. Yager (2007), Seasonal variations in the Amazon plume-related atmospheric carbon sink, *Global Biogeochem. Cycles*, *21*, GB3014, doi:10.1029/2006GB002831.
Didden, N., and F. Schott (1993), Eddies in the North Brazil Current retroflection region observed by Geosat altimetry, *J. Geophys. Res.*, *98*(C11), 20,121–20,131.
DOE (1994), *Handbook of Methods for the Analysis of the Various Parameters of the Carbon Dioxide System in Sea Water*, edited by A. G. Dickson and C. Goyet, Oak Ridge Natl. Lab., Carbon Dioxide Inf. Anal. Cent., Oak Ridge, Tenn.
Edmond, J. M. (1970), High precision determination of titration alkalinity and total carbon dioxide content of seawater by potentiometric titration, *Deep Sea Res. Oceanogr. Abstr.*, *17*(4), 737–750.
Emery, W. J., W. G. Lee, and L. Magaard (1984), Geographic and seasonal distributions of Brunt-Väisälä frequency and rossby radii in the North Pacific and North Atlantic, *J. Phys. Oceanogr.*, *14*, 294–317.
Fratantoni, D. M., and D. A. Glickson (2001), North Brazil Current ring generation and evolution observed with SeaWiFS, *J. Phys. Oceanogr.*, *32*, 1058–1074.
Goyet, C., R. Adams, and G. Eischeid (1998), Observations of the CO_2 system properties in the tropical Atlantic Ocean, *Mar. Chem.*, *60*(1–2), 49–61.
Hu, C., E. T. Montgomery, R. W. Schmitt, and F. E. Muller-Karger (2004), The dispersal of the Amazon and Orinoco River water in the tropical Atlantic and Caribbean Sea: Observation from space and S-PALACE floats, *Deep Sea Res., Part II*, *51*, 1151–1171.
Körtzinger, A. (2003), A significant sink of CO_2 in the tropical Atlantic Ocean associated with the Amazon River plume, *Geophys. Res. Lett.*, *30*(24), 2287, doi:2210.1029/2003GL018841.
Lefèvre, N. (2009), Low CO_2 concentrations in the Gulf of Guinea during the upwelling season in 2006, *Mar. Chem.*, *113*, 93–101.
Lefèvre, N., and A. H. Taylor (2002), Estimating pCO_2 from sea surface temperatures in the Atlantic gyres, *Deep Sea Res., Part I*, *49*, 539–554.
Lefèvre, N., G. Moore, J. Aiken, A. Watson, D. Cooper, and R. Ling (1998), Variability of pCO_2 in the tropical Atlantic in 1995, *J. Geophys. Res.*, *103*(C3), 5623–5634.
Lefèvre, N., A. J. Watson, A. Olsen, A. F. Rios, F. F. Perez, and T. Johannessen (2004), A decrease in the sink for atmospheric CO_2 in the North Atlantic, *Geophys. Res. Lett.*, *31*, L07306, doi:10.1029/2003GL018957.
Lefèvre, N., D. Diverrès, and F. Gallois (2010), Origin of CO_2 undersaturation in the western tropical Atlantic, *Tellus, Ser. B*, *62*(5), 595–607.
Lefèvre, N., G. Caniaux, S. Janicot, and A. K. Gueye (2013), Increased CO_2 outgassing in February-May 2010 in the tropical Atlantic following the 2009 Pacific El Niño, *J. Geophys. Res.*, *118*, 1645–1657.
Lumpkin, R., and S. L. Garzoli (2005), Near-Surface circulation in the Tropical Atlantic Ocean, *Deep Sea Res., Part I*, *52*, 495–518.
Lumpkin, R., and S. L. Garzoli (2011), Interannual to decadal changes in the western South Atlantic's surface circulation, *J. Geophys. Res.*, *116*, C01014, doi:10.1029/2010JC006285.
Mayorga, E., A. K. Aufdenkampe, C. A. Masiello, A. V. Krusche, J. I. Hedges, P. D. Quay, J. E. Richey, and T. A. Brown (2005), Young organic matter as a source of carbon dioxide outgassing from Amazonian rivers, *Nature*, *436*, 538–541.
McKinley, G. A., A. R. Fay, T. Takahashi, and N. Metzl (2011), Convergence of armospheric and North Atlantic carbon dioxide trends on multidecadal timescales, *Nat. Geosci.*, *4*, 606–610, doi:10.1038/NGEO1193.
Niiler, P. P., N. A. Maximenko, G. G. Panteleev, T. Yamagata, D. B. Olson (2003), Near-surface dynamical structure of the Kuroshio Extension, *J. Geophys. Res.*, *108*(C6), 3193, doi: 10.1029/2002JC001461.
Olsen, A., R. G. J. Bellerby, T. Johannessen, A. Omar, and I. Skjelvan (2003), Interannual variability in the wintertime air-sea flux of carbon dioxide in the northern North Atlantic 1981–2001, *Deep Sea Res., Part I*, *50*, 1323–1338.

Oudot, C., and C. Andrié (1986), Variabilité des pressions partielles de CO_2 océanique et atmosphérique dans l'Atlantique tropical, *Oceanol. Acta*, *9*(2), 169–177.
Oudot, C., J. F. Ternon, and J. Lecomte (1995), Measurements of atmospheric and oceanic CO_2 in the tropical Atlantic: 10 years after the 1982–1984 FOCAL cruises, *Tellus, Ser. B*, *47*, 70–85.
Padin, X. A., et al. (2009), Air-sea CO_2 fluxes in the Atlantic as measured during the FICARAM cruises, *Biogeosci. Discuss.*, *6*, 5589–5622.
Park, G.-H., and R. Wanninkhof (2012), A large increase of the CO_2 sink in the western tropical North Atlantic from 2002 to 2009, *J. Geophys. Res.*, *117*, C080029, doi:10.1029/2011JC007803.
Park, G.-H., R. Wanninkhof, S. C. Doney, T. Takahashi, K. Lee, R. A. Feely, C. L. Sabine, J. Triñanes, and I. D. Lima (2010), Variability of global net sea-air CO_2 fluxes over the last three decades using empirical relationships, *Tellus, Ser. B*, *62*, 352–368.
Peterson, R. G., and L. Stramma (1990), Upper-level circulation in the South Atlantic Ocean, *Prog. Oceanogr.*, *26*, 1–73.
Philander, S. G. H., and R. C. Pacanowski (1986), A model of the seasonal cycle in the tropical Atlantic Ocean, *J. Geophys. Res.*, *91*(C12), 14,192–14,206.
Pierrot, D., C. Neill, K. Sullivan, R. Castle, R. Wanninkhof, H. Lüger, T. Johannessen, A. Olsen, R. A. Feely, and C. E. Cosca (2009), Recommendations for autonomous underway pCO_2 measuring systems and data-reduction routines, *Deep Sea Res., Part II*, *56*, 512–522.
Richey, J. E., J. M. Melack, A. K. Aufdenkampe, V. M. Ballester, and L. L. Hess (2002), Outgassing from Amazonian rivers and wetlands as a large tropical source of atmospheric CO_2, *Nature*, *416*, 617–620.
Rios, A., et al. (2005), Carbon dioxide, hydrographic, and chemical data obtained during the R/V Maurice Ewing Cruise in the Atlantic Ocean (WOCE section A17, 4 January21 - March 1994), *Rep. ORNL/CDIAC-148, NDP-084*, Carbon Dioxide Inf. Anal. Cent., Oak Ridge Natl. Lab., U.S. Dep. of Energy, Oak Ridge, Tenn.
Schott, F. A., L. Stramma, and J. Fischer (1995), The warm water inflow into the western tropical Atlantic boundary regime, spring 1994, *J. Geophys. Res.*, *100*(C12), 24,745–24,760.
Schott, F. A., J. Fischer, and L. Stramma (1998), Transports and pathways of the upper-layer circulation in the western tropical Atlantic, *J. Phys. Oceanogr.*, *28*, 1904–1928.
Silveira, I. C. A., L. B. Miranda, and W. S. Brown (1994), On the origins of the North Brazil Current, *J. Geophys. Res.*, *99*(C11), 22,501–22,512.
Stephens, M. P., G. Samuels, D. B. Olson, and R. A. Fine (1995), Sea-air flux of CO_2 in the North Pacific using shipboard and satellite data, *J. Geophys. Res.*, *100*(C7), 13,571–13,583.
Stramma, L., and F. Schott (1999), The mean flow field of the tropical Atlantic Ocean, *Deep Sea Res., Part II*, *46*, 279–303.
Stramma, L., S. Juttl, and J. Schafstall (2005), Water masses and currents in the upper tropical northeast Atlantic off northwest Africa, *J. Geophys. Res.*, *110*, C12006, doi:10.1029/2005JC002939.
Subramaniam, A., et al. (2008), Amazon River enhances diazotrophy and carbon sequestration in the tropical North Atlantic Ocean, *Proc. Natl. Acad. Sci.*, *105*(30), 10,460–10,465.
Sweeney, C., E. Gloor, A. R. Jacobson, R. M. Key, G. McKinley, J. L. Sarmiento, and R. Wanninkhof (2007), Constraining global air-sea gas exchange for CO_2 with recent bomb 14C measurements, *Global Biogeochem. Cycles*, *21*, GB2015, doi:10.1029/2006GB002784.
Takahashi, T., et al. (2009), Climatological mean and decadal change in surface ocean pCO_2, and net sea-air CO_2 flux over the global oceans, *Deep Sea Res., Part II*, *56*, 554–577, doi:10.1016/j.dsr1012.2008.1012.1009.
Ternon, J. F., C. Oudot, A. Dessier, and D. Diverrès (2000), A seasonal tropical sink for atmospheric CO_2 in the Atlantic ocean: The role of the Amazon River discharge, *Mar. Chem.*, *68*(3), 183–201.
Urbano, D. F., M. Jochum, and I. C. A. Da Silveira (2006), Rediscovering the second core of the Atlantic NECC, *Ocean Modell.*, *12*(1–2), 1–15.
Urbano, D. F., R. A. F. De Almeida, and P. Nobre (2008), Equatorial Undercurrent and North Equatorial Countercurrent at 38oW: A new perspective from direct velocity data, *J. Geophys. Res.*, *113*, C04041, doi:10.1029/2007JC004215.
Wanninkhof, R., and J. Hendee (1991), Carbon dioxide, hydrographic and chemical data obtained during the R/V Malcom Baldrige South Atlantic OACES/CO_2 cruise, WOCE section A16S (11 July-02 September 1991), edited by O. R. N. L., Carbon Dioxide Inf. Anal. Cent., U.S. Dep. Energy, Oak Ridge, Tenn. [Available at http://cdiac.ornl.gov/ftp/oceans/OACES91_A16S/. doi: 10.3334/ CDIAC/ otg.WOCE_ OACES91_A16S.]
Wanninkhof, R., R. D. Castle, and J. Shannahoff (2008), Underway pCO_2 measurements aboard the R/V Ronald H. Brown during the 2002 cruises, edited by O. R. N. L., Carbon Dioxide Inf. Anal. Cent., U.S. Dep. of Energy, Oak Ridge, Tenn, doi:10.3334/CDIAC/otg.VOS_RB_2002.
Weiss, R. F. (1974), CO_2 in water and seawater: The solubility of a non-ideal gas, *Mar. Chem.*, *2*, 203–215.
Weiss, R. F., F. A. Van Woy, and P. K. Salameh (1992), Surface water and atmospheric carbon dioxide and nitrous oxide observations by shipboard automated gas chromatography: Results from expeditions between 1977 and 1990, *Rep. ORNL/CDIAC-59*, 144 pp., Oak Ridge Natl. Lab., Oak Ridge, Tenn.
Wilson, W. E., E. Johns, and S. L. Garzoli (2002), Velocity structure of North Brazil Current rings, *Geophys. Res. Lett.*, *29*(8), 1273, doi:10.1029/2001GL013869..
Xie, P., J. E. Janoviak, P. A. Arkin, R. F. Adler, A. Gruber, R. Ferraro, G. J. Huffman, and S. Curtis (2003), GPCP pentad precipitation analyses: An experimental dataset based on gauge observations and satellite estimates, *J. Clim.*, *16*, 2197–2214.